

Study of the flow around a cylinder from the subcritical to supercritical regimes

Xian-tao Zhang^{1a}, Zhi-yu Li¹, Shi-xiao Fu^{*1}, Muk chen Ong² and Ying Chen¹

¹State Key Laboratory of Ocean Engineering, Min Hang District, Dong Chuan Road No.800, Shanghai, 200240, China

²Norwegian Marine Technology Research Institute (MARINTEK), NO-7450 Trondheim, Norway

(Received May 27, 2014, Revised August 22, 2014, Accepted August 25, 2014)

Abstract. The objective of the present simulations is to evaluate the applicability of the standard k- ϵ turbulence model in engineering practice in the subcritical to supercritical flow regimes. Two-dimensional numerical simulations of flow around a circular cylinder at $Re=1\times 10^5$, 5×10^5 and 1×10^6 , had been performed using Unsteady Reynolds-Averaged Navier Stokes (URANS) equations with the standard k- ϵ turbulence model. Solution verification had been studied by evaluating grid and time step size convergence. For each Reynolds number, several meshes with different grid and time step size resolutions were chosen to calculate the hydrodynamic quantities such as the time-averaged drag coefficient, root-mean square value of lift coefficient, Strouhal number, the coefficient of pressure on the downstream point of the cylinder, the separation angle. By comparing the values of these quantities of adjacent grid or time step size resolutions, convergence study has been performed. Solution validation is obtained by comparing the converged results with published numerical and experimental data. The deviations of the values of present simulated quantities from those corresponding experimental data become smaller as Reynolds numbers increases from 1×10^5 to 1×10^6 . This may show that the standard k- ϵ model with enhanced wall treatment appears to be applicable for higher Reynolds number turbulence flow.

Keywords: solution verification; validation; cylinder; k- ϵ ; higher Reynolds number

1. Introduction

Flow around a circular cylinder is of great interest for its applications in engineering problems such as vortex-induced vibration on risers and pipelines, inertia and damping forces of columns of platforms or other cylindrical structures. Most of engineering problems are often subject to very high Reynolds numbers, which makes them hard and expensive to carry out experiments. Thus Computational Fluid Dynamics (CFD) becomes a possible tool to substitute the experimental measurement to predict the hydrodynamic quantities of flows around a circular cylinder. However, due to uncertainties in CFD turbulence model, solution verification and validation of the numerical turbulence models need to be carried out before they can be used for engineering applications (Simonsen 2003, Oberkampf and Trucano 2008, Eca and Vaz 2012).

*Corresponding author, Professor, E-mail: zhxter@gmail.com

^a Master student

Most numerical simulations have been performed at relatively low Reynolds numbers ($Re < 1 \times 10^5$). And there are few studies on numerical simulations at high Reynolds numbers ($Re > 1 \times 10^5$) due to the complex nature of the flow. For such high Reynolds number flow, Direct Numerical Simulation seems to be impossible due to the high demands on computational performance. And only few calculated cases can be found in the open literature (Fung 1960, Cheung and Melbourne 1983, Schewe 1983, Catalano *et al.* 2003 and Singh and Mittal 2005). Catalano *et al.* (2003) performed their numerical studies by applying three-dimensional Large Eddy Simulation (3D LES) with wall modeling, as well as Unsteady Reynolds-Averaged Navier Stokes (URANS) method using the standard k - ϵ turbulence model with their own near-wall treatment, for $5 \times 10^5 < Re < 4 \times 10^6$. And they captured the delayed boundary layer separation and reduced drag coefficient after the drag crisis. They made a conclusion that the 3D LES results were more accurate than the URANS results at Reynolds number near 1×10^6 . Also, they mentioned that the 3D LES results were less accurate compared with the experimental results for the grid resolution was insufficient. Singh and Mittal (2005) aimed to find the possible relationship between the drag crisis and the instability of the sheared layer. And they predicted the flow around a circular cylinder using a two-dimensional Large Eddy Simulation (2D LES) method for $300 < Re < 3 \times 10^5$. And their calculations succeeded to capture the drag crisis close to the critical Reynolds number. Also they showed some results of the quantities in the supercritical regimes. Achenbach (1968) and Sumer (2006) carried out the experiments on the flow around a circular cylinder for $1 \times 10^4 < Re < 1 \times 10^7$. And they gave the relative contribution of the friction force to the total drag for circular cylinder as well as the pressure distribution and wall shear stress distribution at different Reynolds numbers for a smooth cylinder. Also they showed the position of the separation point as a function of the Reynolds number for a smooth circular cylinder.

The standard k - ϵ model with wall functions has been adopted to solve high Reynolds number flow around a circular cylinder to obtain the hydrodynamic quantities. Although the standard k - ϵ model has some shortcomings such as it is less effective to obtain the hydrodynamic quantities nearby the drag crisis regime, it is still a desirable tool to high Reynolds number flow calculations for it is less expensive than LES or DNS model. Franke *et al.* (1989) adopted the standard high Reynolds number k - ϵ model provided by Launder and Spalding (1972). Their studies showed that the standard k - ϵ model predicted the flow in the supercritical regimes relatively accurately with strong anisotropic turbulence. Catalano *et al.* (2003) obtained the time-averaged drag coefficient for $Re = 1 \times 10^6, 2 \times 10^6, 4 \times 10^6$, Strouhal number for $Re = 1 \times 10^6$ as well as mean pressure distribution around a circular cylinder for $Re = 1 \times 10^6$ with the standard k - ϵ model with near wall treatment. Ong *et al.* (2009) performed their numerical studies at $Re = 1 \times 10^6, 2 \times 10^6, 3.6 \times 10^6$ using the standard k - ϵ model with wall functions and got the pressure and skin friction coefficient distribution around the circular cylinder. They gave the separation angle of the flow around a circular cylinder and compared the numerical values with published numerical and experimental data. Also three quantities—the time-averaged coefficient of drag forces (C_{Daver}), the root mean square of the coefficient of lift forces (C_{Lrms}), Strouhal number based on the frequency of vortex shedding (St) are obtained and compared with published numerical and experimental data.

The main objective of this paper is to evaluate the applicability of the standard k - ϵ model with enhanced wall treatment to turbulent flow at high Reynolds number. Solution verification and validation of two-dimensional flow around circular cylinder at $Re = 1 \times 10^5, 5 \times 10^5$ and 1×10^6 is carried out. And the present numerical results are compared with published numerical and experimental results.

2. Mathematical formulations and numerical methods

2.1 Mathematical formulations

The mathematical formulations are as follows.

$$\frac{\partial u_i}{\partial x_i} = 0 \quad (1)$$

$$\frac{\partial u_i}{\partial t} + u_j \frac{\partial u_i}{\partial x_j} = -\frac{1}{\rho} \left(\frac{\partial p}{\partial x_i} \right) + \nu \frac{\partial^2 u_i}{\partial x_j^2} - \overline{\partial u_i' u_j'} \quad (2)$$

$$-\overline{\partial u_i' u_j'} = \nu_T \left(\frac{\partial u_i}{\partial x_j} + \frac{\partial u_j}{\partial x_i} \right) - \frac{2}{3} k \delta_{ij} \quad (3)$$

$$\frac{\partial k}{\partial t} + u_j \frac{\partial k}{\partial x_j} = \frac{\partial}{\partial x_j} \left(\frac{\nu_T}{\sigma_k} \frac{\partial k}{\partial x_j} \right) + \nu_T \left(\frac{\partial u_i}{\partial x_j} + \frac{\partial u_j}{\partial x_i} \right) \frac{\partial u_i}{\partial x_j} - \varepsilon \quad (4)$$

$$\frac{\partial \varepsilon}{\partial t} + u_j \frac{\partial \varepsilon}{\partial x_j} = \frac{\partial}{\partial x_j} \left(\frac{\nu_T}{\sigma_\varepsilon} \frac{\partial \varepsilon}{\partial x_j} \right) + C_1 \frac{\varepsilon}{k} - \nu_T \left(\frac{\partial u_i}{\partial x_j} + \frac{\partial u_j}{\partial x_i} \right) \frac{\partial u_i}{\partial x_j} - C_2 \frac{\varepsilon^2}{k} \quad (5)$$

where $i, j=1, 2$. x_1 and x_2 denotes the horizontal and vertical directions, respectively; u_1 and u_2 are the corresponding mean velocity components. $\overline{u_i' u_j'}$ is the Reynolds stress components. u_i' denotes the fluctuating part of the velocity; p is the dynamic pressure; ρ is the density of the fluid; k is the turbulent kinetic energy; δ_{ij} is the Kronecker delta function; ε is the dissipation rate; $\nu_T = C_\mu (k^2 / \varepsilon)$. The values of the model coefficients are as follows:

$$C_1=1.44, C_2=1.92, C_\mu=0.09, \sigma_k=1.0, \sigma_\varepsilon=1.3$$

For the standard k- ε turbulence model, 'Enhanced Wall Treatment' (Fluent guide 2006) is chosen as the near-wall treatment. Enhanced wall treatment is a near-wall modeling method which combines a two-layer model with enhanced wall functions. The near wall treatment will retain the accuracy of the standard two layer approach for fine near-wall meshes. In the meantime, this method will not significantly reduce the accuracy for wall-function meshes.

2.1.1 Two layer model for enhanced wall treatment

The two-layer approach is used to specify both ε and the turbulent viscosity in the near-wall cells. And the whole domain is divided into a viscosity-affected region and a fully-turbulent region, which is defined as the following Reynolds number

$$\text{Re}_y = \frac{\rho y \sqrt{k}}{\mu} \quad (6)$$

where, y is the distance to the nearest wall. The standard k- ε model are employed as $\text{Re}_y > 200$. While the one-equation model is employed for $\text{Re}_y < 200$. For the one-equation model, with

momentum equations and the k equation being identical to Eqs. (2) and (4) in the standard k - ε model, the turbulent kinematic viscosity $\nu_{T,2layer}$ is computed according to Eqs. (7) and (8)

$$\nu_{T,2layer} = \rho C_{\mu} l_{\mu} \sqrt{k} \quad (7)$$

$$l_{\mu} = y C_l^* (1 - e^{-Re_y/A_{\mu}}) \quad (8)$$

The two-layer definition is smoothly blended with high-Reynolds number ν_T definition from outer region by $\nu_{T,enh}$ as shown in Eqs. (9) and (10)

$$\nu_{T,enh} = \lambda_{\varepsilon} \nu_t + (1 - \lambda_{\varepsilon}) \nu_{t,2layer} \quad (9)$$

$$\lambda_{\varepsilon} = \frac{1}{2} [1 + \tanh(\frac{Re_y - 200}{A})] \quad (10)$$

$$A = \frac{\Delta Re_y}{\tanh(0.98)} \quad (11)$$

ΔRe_y would be given a value that is between 5% and 20% of 200. The blending function λ_{ε} is applied to make sure of solution convergence when the k - ε solution in the outer layer does not match with the two-layer formulation. In the viscosity-affected near-wall region, the ε field is calculated by Eqs. (12) and (13)

$$\varepsilon = \frac{k^{3/2}}{l_{\varepsilon}} \quad (12)$$

$$l_{\varepsilon} = y C_l^* (1 - e^{-Re_y/A_{\varepsilon}}) \quad (13)$$

The constants in Eqs. (8) and (13) are given as follows

$$A_{\mu} = 70, A_{\varepsilon} = 2C_l^*, C_l^* = kC_{\mu}^{-3/4} \quad (14)$$

2.1.2 Enhanced wall functions

u^+ , which is used to blend the linear and logarithmic laws-of-the-wall, is given as follows

$$u^+ = e^{\Gamma} u_{lam}^+ + e^{1/\Gamma} u_{turb}^+ \quad (15)$$

The blending function is given by

$$\Gamma = -\frac{a(y^+)^4}{1 + b(y^+)} \quad (16)$$

where $a=0.05$ and $b=1$. Similarly

$$\frac{du^+}{dy^+} = e^{\Gamma} \frac{du_{lam}^+}{dy^+} + e^{1/\Gamma} \frac{du_{turb}^+}{dy^+} \quad (17)$$

The enhanced turbulent laws-of-the-wall for compressible flow with gradients is given as follows

$$\frac{du_{turb}^+}{dy^+} = \frac{1}{ky^+} S^{1/2} \quad (18)$$

where

$$S = \begin{cases} 1 + \alpha y^+, & \text{for } y^+ < y_s^+ \\ 1 + \alpha y_s^+, & \text{for } y^+ \geq y_s^+ \end{cases} \quad (19)$$

$$\alpha = \frac{v_w}{\tau_w u^*} \frac{dp}{dx} = \frac{\mu}{\rho^2 (u^*)^3} \frac{dp}{dx} \quad (20)$$

where y^+ is the location where the log-law slope will remain fixed. The laminar law-of-the-wall is determined from the following formulation

$$\frac{du_{lam}^+}{dy^+} = 1 + \alpha y^+ \quad (21)$$

2.2 Numerical methods

The time discretization technique is second order implicit. For the space discretization technique, ‘PRESTO!’ is for the pressure; ‘Second Order Upwind’ is for Momentum, Turbulent Kinetic Energy and Specific Dissipation Rate. So the accuracy of time discretization, the space discretization of the continuity and momentum equations and the discretization of the turbulent quantities transport equations are all second order. The interpolation schemes (Trapezoidal method) applied in the post-processing of the data is first order.

3. Computational overview

3.1 Computational domain and boundary conditions

The computational domain for all of the simulations is as following:

The boundary conditions are set as:

(1) Uniform flow is prescribed at the inlet with $u_1=U_\infty$, $u_2=0$. And U_∞ is determined by the Reynolds number $Re=\rho U_\infty D/\mu$. The inlet boundary is set as ‘Velocity-inlet’. The turbulence specification method is chosen as ‘Intensity and Hydraulic Diameter’. The turbulence intensity (I) is estimated from the following formula derived from an empirical correlation for pipe flows:

$$I = 0.16(Re_{D_H})^{-1/8} \quad (22)$$

where Re_{D_H} is the Reynolds number based on the hydraulic diameter (D_H). Re_{D_H} is defined as

$$\text{Re}_{D_H} = \rho U_\infty D_H / \mu \quad (23)$$

The values of turbulence intensity (I) and hydraulic diameter (D_H) for three different Reynolds numbers are listed in Table 1.

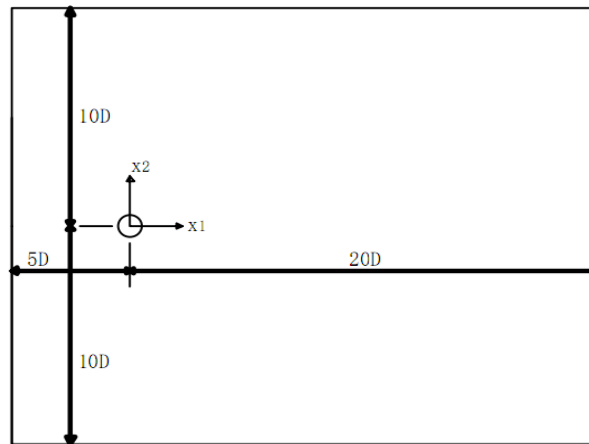


Fig. 1 The computational domain

Table 1 Values of turbulence intensity and hydraulic diameter

Re	Turbulence Intensity	Hydraulic Diameter
1×10^5	3.79%	D
5×10^5	3.10%	D
1×10^6	2.85%	D

* D means the diameter of the circular cylinder

(2) The outlet boundary is set as ‘pressure-outlet’. And we choose turbulence specification method as ‘Intensity and Hydraulic Diameter’. The values of backflow turbulence intensity and backflow hydraulic diameter are the same as those of the inlet boundary.

(3) The cylinder boundary is set as ‘wall’ with no-slip condition for velocity components and zero normal pressure gradients.

(4) The up-external boundary and down-external boundary are set as ‘symmetry’.

3.2 Grid overview

For each Reynolds number, 3 different meshes and 3 different time steps with the combination of 6 calculation cases are carried out. Detailed information about the meshes is listed in Table 2.

Table2 Meshes for different Re

Re	Grid	Nc	Nt	nodes	l/w
1×10^5	grid1	280	70	39k	20
	grid2	368	92	68k	20
	grid3	424	106	90k	20
5×10^5	grid4	340	85	61k	70
	grid5	444	111	99k	70
	grid6	480	120	110k	70
	grid7	512	128	132k	70
1×10^6	grid8	544	138	147k	70
	grid9	340	85	58K	132
	grid10	444	111	96k	132
	grid11	480	122	111k	132
	grid12	512	128	132K	132
	grid13	544	140	148k	132

*Note: Nc=number of nodes in the cylinder circumferential direction in the core region ; Nt=number of nodes in cylinder wall normal direction in the core region; l/w =ratio of length to width for the nearest element to the cylinder

Fig. 2 shows some pictures of the meshes.

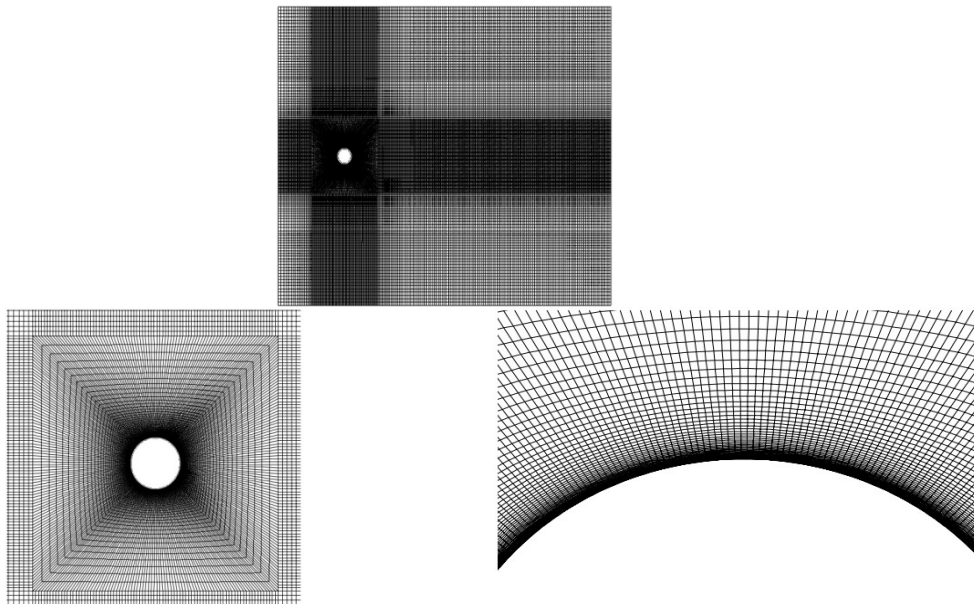


Fig. 2 The computational meshes

4. Results and discussions

4.1 Grid and time step size convergence

Three quantities—the time-averaged drag coefficient (C_{Daver}), root-mean square value of lift coefficient (C_{Lrms}), Strouhal number (St) are considered in the convergence studies. Fluent two-dimensional double precision (2ddp) version is chosen for the calculation. And the maximum digit of the decimal effective digital is 16, which means the machine round-off error is about 1×10^{-16} , so the influence of the machine round-off error can be neglected. The iterative error is set at 1×10^{-6} . It is assumed that the major error is the discretization error. The effects of grid and time step size resolution on the calculated results are evaluated through convergence studies.

4.1.1 Grid convergence

Table 3~5 show the grid convergence studies for three different Reynolds numbers at 1×10^5 , 5×10^5 and 1×10^6 .

We can find from table3 that for $Re=1 \times 10^5$, the relative change of C_{Daver} and St is within 5% for three different meshes. Note that the relative change of C_{Lrms} between grid1 and grid2 is 9.096%, larger than 5%. However, by increasing the number of nodes from grid2 to grid3, the relative change reaches to 4.823%, less than 5%. This indicates that the grid convergence is achieved as the meshes become fine. For $Re=5 \times 10^5$, the relative changes are also within 5% for five different meshes. However, as the grids become finer, the relative changes of the three quantities seem to become non-monotonic. As indicated by Eca and Vaz (2012), This may due to the grid convergences performing in an oscillating way instead of a steadily monotonic way. Eca and Vaz (2012) summarized the calculated properties submitted on the workshop on verification and validation of CFD for workshop flows including the flow around a smooth circular cylinder. They find that for some Reynolds number such as $Re=1 \times 10^5$ and $Re=1 \times 10^5$, the convergence is non-monotonic in space, which demonstrates the difficulties to assess and control the numerical uncertainty of complex turbulent flow. Although the relative changes for three quantities are oscillating as the grids become finer, most of them are even less than 1% and all of them are within 5%. So the calculated grids results are reasonable and acceptable in a general sense. Similar results are for $Re=1 \times 10^6$.

4.1.2 Time step size convergence

Tables 6-8 show the time step size convergence studies for three different Reynolds numbers at 1×10^5 , 5×10^5 and 1×10^6 .

We can find from table6 that for grid3, the relative change of C_{Daver} , C_{Lrms} , St is within 5% for five different time steps. This indicates that the numerical results are not sensitive for time step size above. This means the time step size convergence for $Re=1 \times 10^5$ is achieved. However the time step size convergence performs in a non-monotonic way, which is also indicated by Eca and Vaz (2012). This may due to the randomness and complexity of the turbulent flow around a circular cylinder at high Reynolds numbers (for example, $Re \geq 1 \times 10^5$).

For $Re=5 \times 10^5$, we find that for grid7 the relative change of C_{Daver} is within 5% for different time steps. And the relative change of C_{Lrms} between t1 and t2 is 7.306%, with time step size reducing to t3 and t4, the relative change reaches to 2.082% and 2.693% respectively, within 5%. The relative change of St between t1, t2 and t3 is within 5%. However, with time step size reducing to t4, the relative error even reaches to 9.939%, much more than 5%. This may tell us that the values of time

step size have different effects on C_{Lrms} and St . And due to the complexity of turbulent flow and the defect of the numerical model, it seems hard to ensure the three quantities to converge in a similar way. Similar results are for $Re=1 \times 10^6$.

In this paper, the calculated results of grid3_t2, grid7_t2, grid12_t2 are chosen as the final results for the following analysis.

4.2 Analysis of quantities

4.2.1 Comparison of C_{Daver} , C_{Lrms} and St

Table 9 shows the comparison of the present results of C_{Daver} , C_{Lrms} and St with published numerical and experimental data.

For $Re=1 \times 10^5$, the present calculated results of C_{Daver} , C_{Lrms} and St are all outside the range of experimental data from Achenbach. Similar results are for $Re=5 \times 10^5$. This may be due to the fact that the standard k- ϵ model is developed for fully turbulent flow. For $Re=1 \times 10^5$, the flow in the boundary layer separation is still laminar although the wake is completely turbulent. This may lead to the k- ϵ model together with enhanced wall treatment depicting the flow in a less accurate and effective way. With Reynolds number increasing to 5×10^5 , the boundary layer separation is becoming turbulent. And the boundary layer becomes partly laminar partly turbulent. But the laminar boundary takes a larger proportion than the turbulent boundary. So the calculation results for $Re=5 \times 10^5$ is also unsatisfactory. As Reynolds number increases to 1×10^6 , although the flow is still in the supercritical regime, the turbulent boundary layer becomes dominant compared with the laminar boundary layer. This makes the flow condition approaches to the state where the standard k- ϵ model is proper and relatively accurate. And the calculated results for $Re=1 \times 10^6$ are mostly within the range of experimental data.

For $Re=1 \times 10^6$, the present results, especially the important parameter C_{Daver} , agree well with Achenbach's experiment (Sumer and Fredsoe 2006), which are superior to previous results by 3D LES and standard k- ϵ (Catalano *et al.* 2003), 2D LES (Singh and Mittal 2005) and standard k- ϵ (Ong *et al.* 2009). Besides, the present results are different from those by Ong *et al.* (2009) and Catalano *et al.* (2003) using the same turbulence model. Especially larger differences appear for the C_{Daver} and C_{Lrms} . This may be due to the different implementations of the wall functions. Compared with Singh and Mittal (2005) 2D LES, the calculated results of Catalano *et al.* (2003) 3D LES agrees better with the experimental results, which may be due to the fact that effects from the spanwise secondary flow are not considered in the 2D simulation (Mittal and Balachandar 1995). Also we can make conclusions that the standard k- ϵ model with enhanced wall treatment has advantages over calculating the high-Reynolds-number ($Re=1 \times 10^6$) flow problems with more accurate results, compared with 2D LES and 3D LES model.

4.2.2 Analysis of the quantity C_{pb}

C_{pb} is the time-averaged pressure coefficient at $\theta=180^\circ$ location downstream of the cylinder and can be defined as

$$C_{pb} = \frac{P_{cb} - P_\infty}{0.5 \rho U_\infty^2} \quad (24)$$

For the three Reynolds number $Re=1 \times 10^5$, 5×10^5 and 1×10^6 , the wake is all turbulent. So the accurate calculation of pressure coefficient of the downstream position of cylinder is an indication

for the accuracy of the simulation of the flow.

Table 3 Grid convergence results for $t_1=0.0408s$ at $Re=1 \times 10^5$

Grid	Nodes	C_{Daver}	Relative change	C_{Lrms}	Relative change	St	Relative change
grid1_t1	39000	0.49108	---	0.09169	---	0.28226	---
grid2_t1	68000	0.48728	0.774%	0.08335	9.096%	0.28447	0.783%
grid3_t1	90000	0.48721	0.014%	0.08737	4.823%	0.28336	0.390%

Table 4 Grid convergence results for $t_1=0.0039s$ at $Re=5 \times 10^5$

Grid	Nodes	C_{Daver}	Relative change	C_{Lrms}	Relative change	St	Relative change
grid4_t1	61000	0.39069	---	0.06366	---	0.29008	---
grid5_t1	99000	0.39048	0.056%	0.06339	0.415%	0.29119	0.383%
grid6_t1	11000	0.39097	0.125%	0.06455	1.834%	0.29058	0.209%
grid7_t1	132000	0.39142	0.115%	0.06543	1.354%	0.28924	0.461%
grid8_t1	147000	0.39193	0.130%	0.06671	1.961%	0.28912	0.041%

Table 5 Grid convergence results for $t_1=0.0026s$ at $Re=1 \times 10^6$

Grid	Nodes	C_{Daver}	Relative change	C_{Lrms}	Relative change	St	Relative change
grid9_t1	58000	0.33839	---	0.04246	---	0.29655	---
grid10_t1	96000	0.33856	0.050%	0.04256	0.222%	0.29655	0
grid11_t1	111000	0.33882	0.077%	0.04328	1.690%	0.29464	0.644%
grid12_t1	132000	0.33897	0.044%	0.04368	0.936%	0.29395	0.654%
grid13_t1	148000	0.33950	0.156%	0.04500	3.012%	0.29400	0.440%

Table 6 Time Step Size convergence results for grid3 at $Re=1 \times 10^5$

Grid	Time step size	C_{Daver}	Relative change	C_{Lrms}	Relative change	St	Relative change
grid3_t1	0.0408	0.48721	---	0.08737	---	0.28336	---
grid3_t2	0.0347	0.48613	0.222%	0.08371	4.186%	0.28205	0.464%
grid3_t3	0.0286	0.48636	0.046%	0.08354	0.211%	0.27479	2.572%
grid3_t4	0.0243	0.48573	0.129%	0.08260	1.126%	0.27474	0.020%
grid3_t5	0.0200	0.48517	0.115%	0.08100	1.938%	0.27535	0.223%

Table 7 Time Step Size convergence results for grid7 at $Re=5 \times 10^5$

Grid	Time step size	C_{Daver}	Relative change	C_{Lrms}	Relative change	St	Relative change
grid7_t1	0.0039	0.39142	---	0.06543	---	0.28924	---
grid7_t2	0.0027	0.38957	0.473%	0.06065	7.306%	0.29202	0.961%
grid7_t3	0.0023	0.38882	0.195%	0.05939	2.082%	0.29056	0.500%
grid7_t4	0.0019	0.39008	0.326%	0.06099	2.693%	0.26168	9.939%

Table 8 Time Step Size convergence results for grid12 at $Re=1 \times 10^6$

Grid	Time step size	C_{Daver}	Relative change	C_{Lrms}	Relative change	St	Relative change
grid12_t1	0.0026	0.33897	---	0.04368	---	0.29395	---
grid12_t2	0.0018	0.33729	0.496%	0.03868	11.447%	0.29626	0.786%
grid12_t3	0.0015	0.33630	0.292%	0.03582	7.394%	0.29699	0.247%
grid12_t4	0.0012	0.33713	0.246%	0.03754	4.782%	0.26597	10.446%

Table 9 Numerical and experimental results at $Re=1\times 10^5$, 5×10^5 and 1×10^6

Re	Cases	C_{Daver}	C_{Lrms}	St
1×10^5 (subcritical)	Present	0.48636	0.08354	0.27479
	Achenbach Exp. (Sumer 2006) and Eca <i>et al.</i> (2012)	1.2~1.3	0.29~0.30	0.20
5×10^5 (supercritical)	Present	0.38957	0.06065	0.29202
	Achenbach Exp. (Sumer 2006)	0.275~0.310	0.02	0.48
1×10^6 (supercritical)	Present	0.33729	0.03868	0.29626
	Catalano <i>et al.</i> 3D LES (2003)	0.31	---	0.35
	Catalano <i>et al.</i> standard k- ϵ (2003)	0.41	---	---
	SP. Singh and S. Mittal 2D LES (2005)	0.591	---	---
	Ong <i>et al.</i> standard k- ϵ (2009)	0.5174	0.0901	0.2823
	Achenbach Exp. (Sumer 2006)	0.35~0.38	0.03~0.15	0.18~0.50

Table 10 is the comparison of present results with published numerical and experimental data.

Table 10 Numerical and experimental result of C_{pb}

Re	Cases	C_{pb}
1×10^5	Present	-0.42464
	Achenbach Exp. (Sumer 2006)	-1.188
5×10^5	Present	-0.31549
	Present	-0.23755
1×10^6	Ong <i>et al.</i> (2009)	-0.59
	Catalano <i>et al.</i> standard k- ϵ (2003)	-0.44
	Catalano <i>et al.</i> 3D LES (2003)	-0.28
	SP. Singh and S. Mittal 2D LES (2005)	-0.83

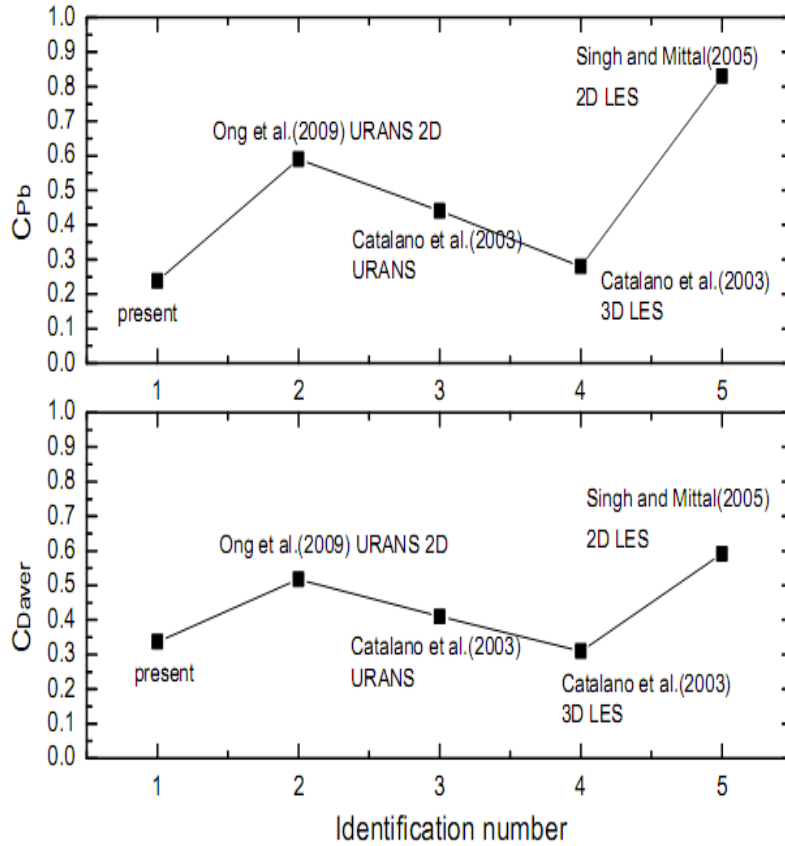


Fig. 3 Results of C_{Daver} and C_{pb} for different numerical simulations

We can find that for $Re=1 \times 10^5$, C_{pb} by present simulation varies a lot with experimental data. This indicates that the $k-\epsilon$ model cannot properly simulate the flow at Reynolds number around 1×10^5 , which agrees with other three quantities— C_{Daver} , C_{Lrms} , St discussed before. For $Re=1 \times 10^6$, the present results of C_{pb} and C_{Daver} are compared with several other numerical simulations as shown in Fig. 3

As shown in Fig. 2, the trend of the values of C_{pb} for different numerical simulations is similar to that of the values of C_{Daver} , which drives us to make the conclusion that the quantity C_{pb} is an effective indication for monitoring the numerical simulations.

4.2.3 Analysis of the separation angle θ_{sep}

At the separation point, the velocity gradient is zero, which indicates that the time-averaged skin friction coefficient C_f is zero. C_f is defined as follows

$$C_f = \frac{\tau}{0.5\rho U_\infty^2} \tag{25}$$

where τ is the tangential wall shear stress.

The prediction of C_f for three different Reynolds number are shown in the Fig. 4.

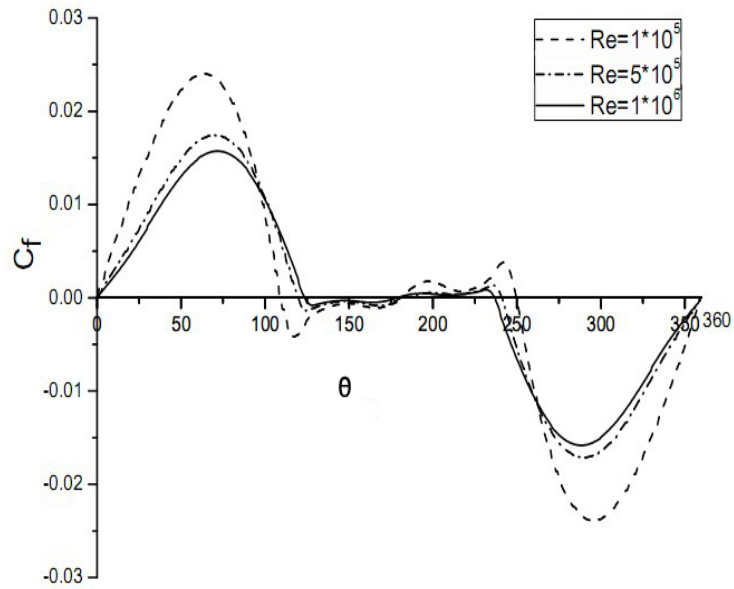


Fig. 4 Present computations of skin friction distribution around the cylinder

Note: the separation angle is defined as the angle clockwise from the stagnant point.

We compare the separation angle (θ) with other simulations and experimental data in the following Table 11.

Table 11 comparison of the separation angle

Re	Cases	Separation angle(degree)
1×10^5	Present	109.2
	Achenbach Exp. (Sumer 2006)	77
5×10^5	Present	119.1
	Achenbach Exp. (Sumer 2006)	141
1×10^6	Present	123.5
	Catalano <i>et al.</i> standard k- ϵ (2003)	111.7
	Catalano <i>et al.</i> 3D LES (2003)	101.4
	Achenbach Exp. (Sumer 2006)	135

We can find from the table 11 that for $Re=1\times 10^5$ and 5×10^5 , the present results of separation angle varies a lot with the experimental data, which is in agreement with the former analysis of the results of the quantities C_{Daver} , C_{Lrms} and St . For Achenbach's experimental data, the separation angle at $Re=5\times 10^5$ is larger than that of the other two Reynolds numbers. This is because flow at $Re=5\times 10^5$ is near the drag crisis regime. However, the present calculated result does not correspond to the fact, which demonstrates that the standard k- ϵ model has the deficit of not capturing the flow characteristics near the drag crisis regime. For $Re=1\times 10^6$, the present result of separation angle is larger than that calculated by Ong *et al.* (2009). This may be due to the different implementations of wall functions. Compared with results by Catalano *et al.* 3D LES (2003), the present simulation using standard k- ϵ model agrees better with experimental data. Also we can make conclusions that as the Reynolds number increases, the deviation of results of present simulations from the experimental data becomes smaller, which indicates that the standard k- ϵ turbulence model is effective for flow problems with high Reynolds number.

Overall, the standard k- ϵ model with enhanced wall treatment appears to show better predictions of turbulent flow around a circular cylinder as the Reynolds numbers get larger from 1×10^5 to 1×10^6 . This indicates that k- ϵ turbulence model will be an effective tool for engineering practice such as simulations of the hydrodynamic conditions of pipeline or risers, not only for its relatively accurate predictions with relatively high calculation speed but also for its accessibility in most commercial CFD software.

5. Conclusions

In this article, the applicability of the standard k- ϵ model in engineering practice in the subcritical to supercritical offshore flow regimes has been studied by simulating flow around a circular cylinder at $Re=1\times 10^5$, 5×10^5 and 1×10^6 . For each Reynolds number, several meshes with different grid and time step size resolutions are chosen in order to study the convergence of the k- ϵ turbulence model. And the converged results are compared with published numerical and experimental data to perform solution validation. The most important conclusions of the article are summarized as follows:

(1) At $Re=1\times 10^5$, grid convergence has been passed in a monotonic way for C_{Daver} , C_{Lrms} and St . The convergence of the time step sizes performs in a non-monotonic way.

(2) At $Re=5\times 10^5$, the grid convergences are obtained with the relative changes performing in an oscillating way instead of a steadily monotonic way. Strouhal number becomes sensitive as the time step size reduces to a rather small value. Proper value of time step size needs to be evaluated for calculation of the hydrodynamic quantities especially for the Strouhal number. At $Re=1\times 10^6$, the results are similar as those at $Re=5\times 10^5$.

(3) At $Re=1\times 10^5$ and $Re=5\times 10^5$, the present calculated results differs a lot from experimental data. At $Re=1\times 10^6$, the present calculated C_{Daver} , C_{Lrms} and St are in a good agreement with the experimental values. However the separation angle differs from the experimental data for all three Reynolds numbers.

(4) The standard k- ϵ model with enhanced wall treatment is not proper for calculating flow problems in subcritical regimes. In supercritical regimes, the turbulence model has the deficit of not capturing flow characteristics near drag crisis point (Re near 5×10^5). But the turbulence model shows better prediction of turbulent flow around a cylinder as Reynolds number increases over drag crisis point in supercritical regime.

(5) The standard k- ϵ model predicts the high-Reynolds-number flow problems with more accurate results, compared with 2D LES model. At $Re=1\times 10^6$, the values of $C_{D_{aver}}$, St and C_{pb} and θ calculated by the standard k- ϵ model are close to those by 3D LES model. However, the former are two-dimensional cases, which saves much calculation time and expense.

Finally, it is truth-worthy to mention that the standard k- ϵ model with enhanced wall treatment is sufficiently applicable for simulating relatively high Reynolds number (Re near 1×10^6) offshore flow for both its relatively accurate predictions with relatively high calculation speed and its accessibility in most commercial CFD software.

References

- Achenbach, E. (1968), "Distribution of local pressure and skin friction around a circular cylinder in cross-flow up to $Re=5\times 10^6$ ", *J. Fluid Mech.*, **34**(4), 625-639.
- Catalano, P., Wang, M., Iaccarino, G. and Moin, P. (2003), "Numerical simulation of the flow around a circular cylinder at high Reynolds numbers", *Int. J. Heat Fluid Fl.*, **24**(4), 463-469.
- Cheung, J.C.K. and Melbourne, W.H. (1983), "Turbulence effects on some aerodynamic parameters of a circular cylinder at supercritical numbers", *J. Wind Eng. Ind. Aerod.*, **14**(1), 399-410.
- Eça, L. and Vaz, G. (2012), "Workshop on verification and validation of CFD for offshore flows", *Proceedings of the ASME 2012 31st International Conference on Ocean, Offshore and Arctic Engineering*, Rio de Janeiro, Brazil, July.
- FLUENT User's Guide (2006), Version 6.3, FLUENT Inc, USA.
- Franke, R., Rodi, W. and Schönung, B. (1989), "Analysis of experimental vortex-shedding data with respect to turbulence modelling", *Proceedings of the 7th Symposium on Turbulent Shear Flows*, Stanford, USA.
- Fung, Y.C. (1960), "Fluctuating lift and drag acting on a cylinder in a flow at supercritical Reynolds numbers", *J. Aeronaut. Sci.*, **27**, 801-814.
- Lauder, B.E. and Spalding, D.B. (1972), *Mathematical models of turbulence*, Academic Press, London.
- Mittal, R. and Balachandar, S. (1995), "Effect of three dimensionality on the lift and drag of nominally two dimensional cylinders", *Phys. Fluids*, **7**(8), 1841-1865.
- Oberkampf, W.L. and Trucano, T.G. (2008), "Verification and validation benchmarks", *Nuclear Eng. Des.*, **238**(3), 716-743.
- Ong, M.C., Utnes, T., Holmedal, L.E., Myrhaug, D. and Pettersen, B. (2009), "Numerical simulation of flow around a smooth circular cylinder at very high Reynolds numbers", *Marine Struct.*, **22**(2), 142-153.
- Schewe, G. (1983), "On the force fluctuations acting on a circular cylinder in crossflow from subcritical up to transcritical Reynolds numbers", *J. Fluid Mech.*, **133**, 265-285.
- Simonsen, C.D. and Stern, F. (2003), "Verification and validation of RANS maneuvering simulation of Esso Osaka: effects of drift and rudder angle on forces and moments", *Comput. Fluids*, **32**(10), 1325-1356.
- Singh, S.P. and Mittal, S. (2005), "Flow past a cylinder: shear layer instability and drag crisis", *Int. J. Numer. Meth. Fl.*, **47**(1), 75-98.
- Sumer, B.M. (2006), *Hydrodynamics around cylindrical structures*, World Scientific.